AIP | Applied Physics Letters

Transparent bulk-size nanocomposites with high inorganic loading

Shi Chen and Romain Gaume

Citation: Applied Physics Letters **107**, 241906 (2015); doi: 10.1063/1.4938001
View online: http://dx.doi.org/10.1063/1.4938001
View Table of Contents: http://scitation.aip.org/content/aip/journal/apl/107/24?ver=pdfcov
Published by the AIP Publishing

Transparent bulk-size nanocomposites with high inorganic loading

Shi Chen[1] and Romain Gaume[1,2,3,a)]
[1]CREOL, College of Optics and Photonics, University of Central Florida, Orlando, Florida 32816, USA
[2]Department of Materials Science and Engineering, University of Central Florida, Orlando, Florida 32816, USA
[3]NanoScience Technology Center, University of Central Florida, Orlando, Florida 32816, USA

(Received 30 September 2015; accepted 2 December 2015; published online 14 December 2015)

With relatively high nanoparticle loading in polymer matrices, hybrid nanocomposites made by colloidal dispersion routes suffer from severe inhomogeneous agglomeration, a phenomenon that deteriorates light transmission even when the refractive indices of the inorganic and organic phases are closely matched. The dispersion of particles in a matrix is of paramount importance to obtain composites of high optical quality. Here, we describe an innovative, yet straightforward method to fabricate monolithic transparent hybrid nanocomposites with very high particle loading and high refractive index mismatch tolerance between the inorganic and organic constituents. We demonstrate 77% transmission at 800 nm in a 2 mm-thick acrylate polymer nanocomposite containing 61 vol. % CaF_2 nanoparticles. Modeling shows that similar performance could easily be obtained with various inorganic phases relevant to a number of photonic applications. © *2015 AIP Publishing LLC*.
[http://dx.doi.org/10.1063/1.4938001]

Nanocomposites, in particular, inorganic-organic hybrids, enable to capitalize on a plethora of available nanoparticles with unique optical properties so as to generate functional devices for lighting,[1,2] display,[3] solar cell,[4,5] laser,[6] magneto-optics,[7] scintillation,[8,9] dentistry,[10] and plasmonics[11,12] applications. Intense research efforts on optical nanocomposites are motivated by the fascinating prospect that composites can assume the optical properties of the inorganic phase and yet be processed with the low-cost, shape versatility, and ease of polymeric materials.

Various routes have been explored to fabricate high-performance optical composites with good transparency. The most general and straightforward approach is based on direct mixing of nanoparticles in a monomer followed by *in-situ* polymerization,[7,13–16] and mostly limited to low inorganic fractions due to poor particle dispersion. Extensive surface chemistry modification[17–20] is often necessary to maintain a compatible polarity and Hamaker constant between the polymer precursor and the nanoparticles in order to facilitate their homogenization. Despite recent and pioneering results on transparent biomimetic artificial nacre[21] with inorganic loadings over 35 vol. %[32] and transmission above 80%, albeit in very thin (25 μm) samples, much development on bulk-size samples with heavy inorganic loading is still difficult. Similarly, physical vapor deposition has also been used to produce nanocomposites films with high loading fractions.[22] Other clever strategies include the use of fluoropolymers in combination with fluoride nanoparticles[23] and sol-gel derived[24] syntheses. Although both approaches can produce nanocomposites with broadly tunable phase ratio and high transparency in the visible, their effectiveness is limited either by cost or oxide materials that can be produced by hydrolysis of a metalorganic precursor.

In this paper, we present a general approach for fabricating transparent monolithic nanocomposites with high inorganic loadings which circumvent the above limitations. Our concept takes advantage of two complementary techniques: (i) the production of high-quality ceramic powder-compacts (so called "green-bodies") used and being developed for the fabrication of transparent laser ceramics[25] and (ii) a polymer impregnation technique. Ceramic green-bodies, made by consolidation of unagglomerated particles, form an open network of interconnected porosity suitable for liquid monomer impregnation as depicted in Figure 1(a). The characteristic of the so-called ceramic open-porosity determines (i) the inorganic loading of the composite once infiltrated by the monomer and (ii) the size of the polymer inclusions which form after *in-situ* polymerization. Thus, the inorganic volume fraction of the nanocomposites can be varied through the use of different green-body forming techniques, including cold-pressing and slip-casting.

In the present study, calcium fluoride nanoparticles were precipitated from commercial calcium nitrate tetrahydrate and sodium fluoride aqueous solutions as described elsewhere.[26] The CaF_2 green-body was formed by cold isostatic pressing at 200 MPa. The monomer was a mixture of polyhydroxydiethoxylate bisphenol-A dimethacrylate (CAS# 24448–20-2) and methacrylic acid ester dodecyl methacrylate (CAS# 90551–76-1) from Ted Pella, Inc. After infiltration of the ceramic green-body, the polymerization was carried out at 52 °C for more than 24 h with benzoyl peroxide as an initiator. Calcium fluoride (CaF_2) and low-viscosity monomers exhibiting low shrinkage upon polymerization were chosen for the proof-of-concept of our approach. After synthesis and dry-compaction of the CaF_2 nanoparticles, the relative density of the green-body (that is, the inorganic loading fraction of the final composite) is found to be 61 vol. % (i.e., 84 wt. %). Figure 1(b) shows the pore-size distribution of a CaF_2 green-body before polymer infiltration and

a)Author to whom correspondence should be addressed. Electronic mail: gaume@ucf.edu

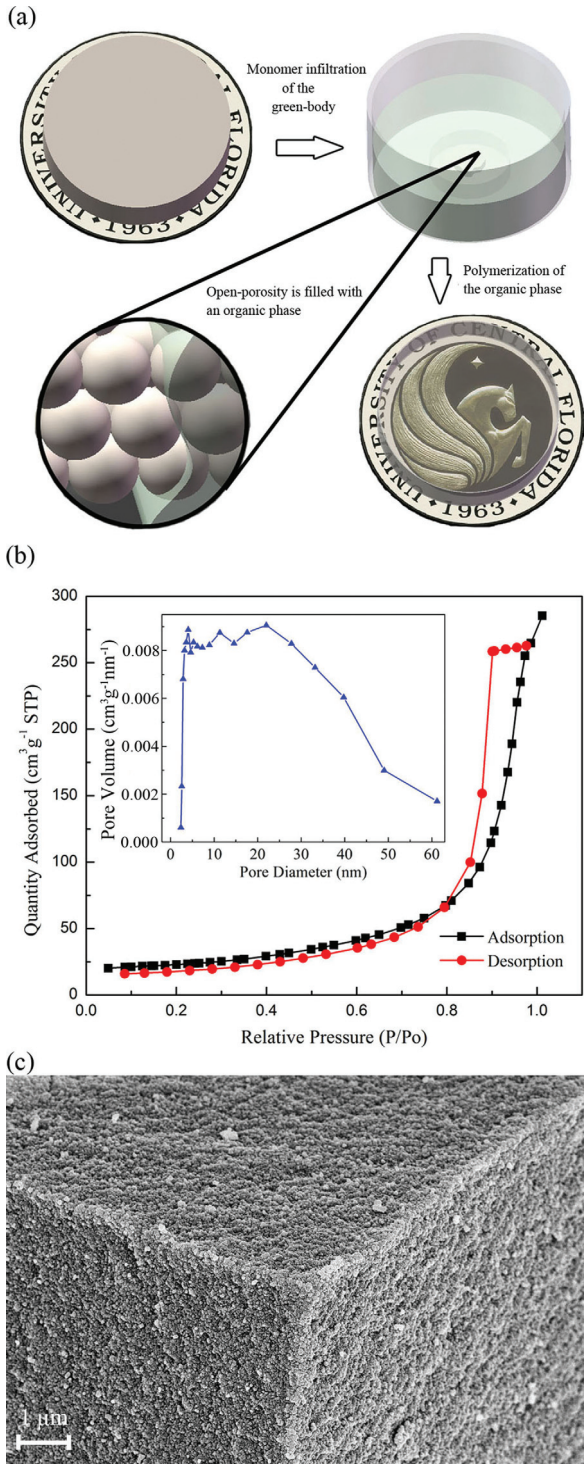

FIG. 1. (a) Fabrication of hybrid nanocomposites by infiltration. (b) Open-porosity of a CaF_2 powder-compact measured by the gas sorption technique and analyzed by the BJH method (inset). (c) SEM of a CaF_2 powder-compact before polymer infiltration.

measured by the nitrogen sorption technique. The size of the pores ranges between 3 and 60 nm with most open-volume formed by 5–20 nm-pores. The Scanning Electron Microscopy (SEM, Zeiss Ultra-55, Jena, Germany) image of Figure 1(c) reveals the open-porosity of the CaF_2 green-body. For a given green-body size and porosity, the viscosity of the monomer highly determines the time required for complete infiltration. Typically, a 2 mm-thick sample with the above pore-size distribution gets fully impregnated by a 10 mPa·s viscous monomer in 10 min while 2 h are necessary when the viscosity is 50 mPa·s. Once fully impregnated, the sample turns transparent and visually disappears from the monomer solution.

Figure 2(a) shows the picture of a 2 mm-thick transparent CaF_2–acrylate nanocomposite obtained after polymerization of the organic phase. The 25 mm-diameter composite (center part of the sample) is surrounded by a polymer cladding. In Figure 2(b), the SEM image of a fracture surface of the composite reveals its microstructure. The low magnification and contrast of the SEM does not permit to discern the organic phase in the composite. However, this image reveals the good homogeneity of the powder-compact and confirms the absence of large porosity.

Further microstructural analyses were performed under Transmission Electron Microscopy (TEM, FEI Tecnai F30, Oregon, USA). To this end, CaF_2-acrylate nanocomposites were milled and welded by a lift-out process in a Focused Ion Beam (FIB, FEI 200, Oregon, USA) equipment. Figure 3(a) shows a side-view of the 10 μm-long, 5 μm-wide, and 182 nm-thick nanocomposite strip sample hence produced. Further milling of the sample, down to a single nanoparticle-thick level could not be achieved with our current instrumental capabilities. The High-Angle Annular Dark-field Scanning Transmission Electron Microscopy (HAAD-STEM) image of the welded composite sample in Figure 3(b) reveals the

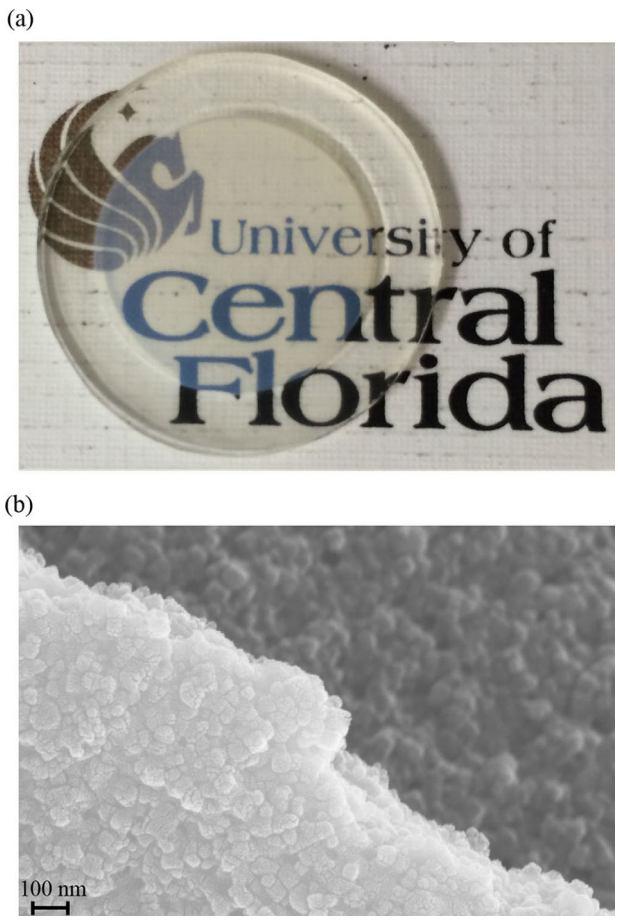

FIG. 2. (a) 25 mm-diameter and 2 mm-thick transparent CaF_2-acrylate nanocomposite sample with 61 vol. % CaF_2 nanoparticles. The refractive index mismatch Δn is 0.065 at 633 nm. (b) SEM image of a fracture surface in a CaF_2-acrylate nanocomposite.

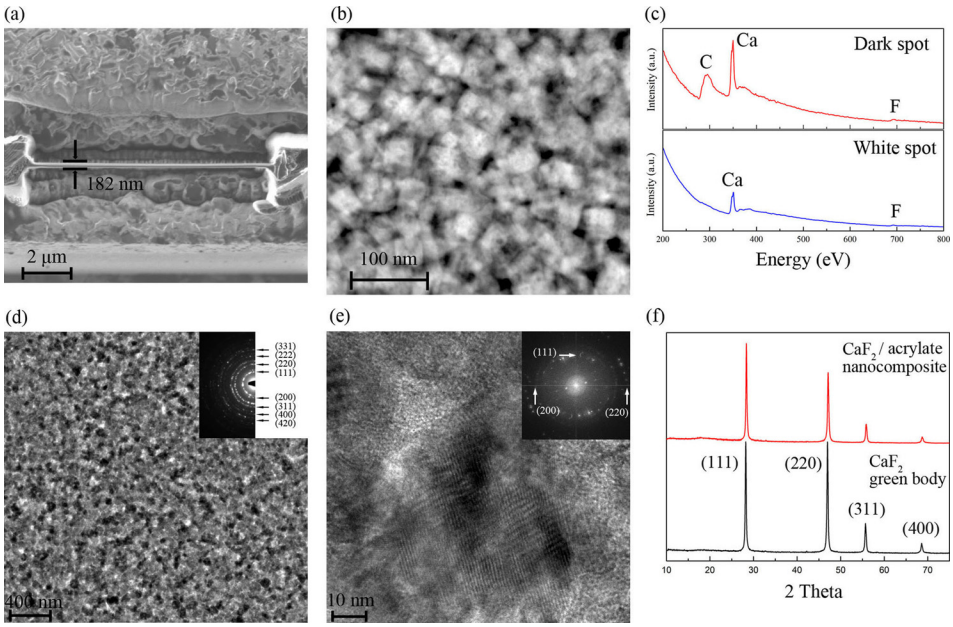

FIG. 3. (a) TEM sample preparation of a CaF_2-acrylate nanocomposite, (b) HAAD-STEM, (c) PEELS, (d) low resolution TEM with indexed SAD in inset, (e) high resolution TEM images with indexed FFT in inset, and (f) XRD of CaF_2 powder-compact and nanocomposite.

distinct contrast between the high-density inorganic phase and low-density polymer phase, a distinction that SEM could not achieve. Parallel Electron Energy-Loss Spectroscopy (PEELS) in Figure 3(c) can further identify the elemental composition of the dark and white areas of the HAAD-STEM image of Figure 3(b) and confirms that the brighter and darker spots are associated to the CaF_2 crystallites and the organic phase, respectively. Figure 3(d) shows a bright-field TEM image, along with the corresponding indexed Selected Area Diffraction (SAD) pattern as an inset, for the 182 nm-thick composite. This SAD pattern exhibits a set of sharp concentric rings which can be well indexed to polycrystalline CaF_2. High-resolution TEM images, such as shown in Figure 3(e), reveal irregularly shaped CaF_2 nanoparticles with sizes ranging from 5 to 20 nm, while in inset the fast Fourier transformation (FFT) pattern shows amorphous feature (halo around the center bright spot), as well as single-crystalline and polycrystalline features that has been indexed to CaF_2. Figure 3(f) gives the structural information for the bulk of CaF_2 powder compact and nanocomposite. The XRD pattern can be indexed with the same atomic planes as in the SAD pattern for CaF_2. There are no noticeable amorphous features in the XRD pattern due to the very strong diffraction signal of the high CaF_2 volume fraction.

In the near infrared (NIR), the refractive index of CaF_2 and of the acrylate polymer differ by about $\Delta n = 6 \times 10^{-2}$ ($\log_{10}\Delta n/n \sim -1.38$). This index mismatch worsens at shorter wavelengths due to the stronger optical dispersion of the polymer in comparison to that of calcium fluoride (Figure 4(a)). In addition, acrylate polymers exhibit optical absorption losses due to high harmonics of C-H vibrations (C-H overtones ν labeled on the figure). While this intrinsic absorption limits the current optical performance of our composites, several strategies, including the use of deuterated and or fluorinated acrylates,[27,28] are known to mitigate this issue.

Based on the optical properties of the individual inorganic and organic phases and the characteristics of the green-body, it is possible to model the expected inline transmittance of nanocomposites using Mie's solution to light scattering.[29–31] The result is shown in Figure 4(b), where best agreement between experimental data (solid line) and the model (dashed line) is obtained for an average polymer inclusion size of $\langle r \rangle = 15$ nm and an inorganic loading fraction of 61 vol. %. These fitting parameters agree reasonably well with the characteristics of the green-body discussed earlier and which are shown in Figure 1(b). This calculation takes into account the measured polymer bulk absorption and refractive index dispersions as shown in Figure 4(a) (dashed line). The grey spindle-shaped area indicates the sensitivity of this calculation to the average polymer inclusion size. The same assumptions, but neglecting polymer absorption, yield the transmission represented by the dotted line. By reducing the absorption loss of the polymer, the experimental transmittance would converge, in the NIR where the effect of scattering is less predominant than at short wavelengths, to a maximum of $T = 93\%$. This value agrees with the transmission, T, resulting from Fresnel reflection losses, R, at the interfaces of a homogenous solid of average index $\tilde{n}$

$$T = (1 - R)^2, \tag{1}$$

$$R = (1 - \tilde{n})^2/(1 + \tilde{n})^2, \tag{2}$$

$$\tilde{n} = 1/2 \times (n_{CaF_2} + n_{polymer}) = 1.475. \tag{3}$$

This model can further be used to predict the inline transmittance of acrylate-based nanocomposites formed with other inorganic phases. For example, Figures 4(c) and 4(d) illustrate the expected scattering cross-section, C_{sca}, and transmittance of acrylate-based composites formed with BaF_2, SiO_2, LaF_3, $LiYF_4$, and KD_2PO_4 (KDP). These calculations assume 61 vol. % inorganic loading, an average 15 nm polymer inclusion size, a nominal polymer bulk absorption of 0.47 cm^{-1} and that, for small particles (<20 nm), the effect of birefringence in non-isotropic crystallites can be neglected in the visible and NIR. However, depending on the actual size of the particles and amount of birefringence, the latter

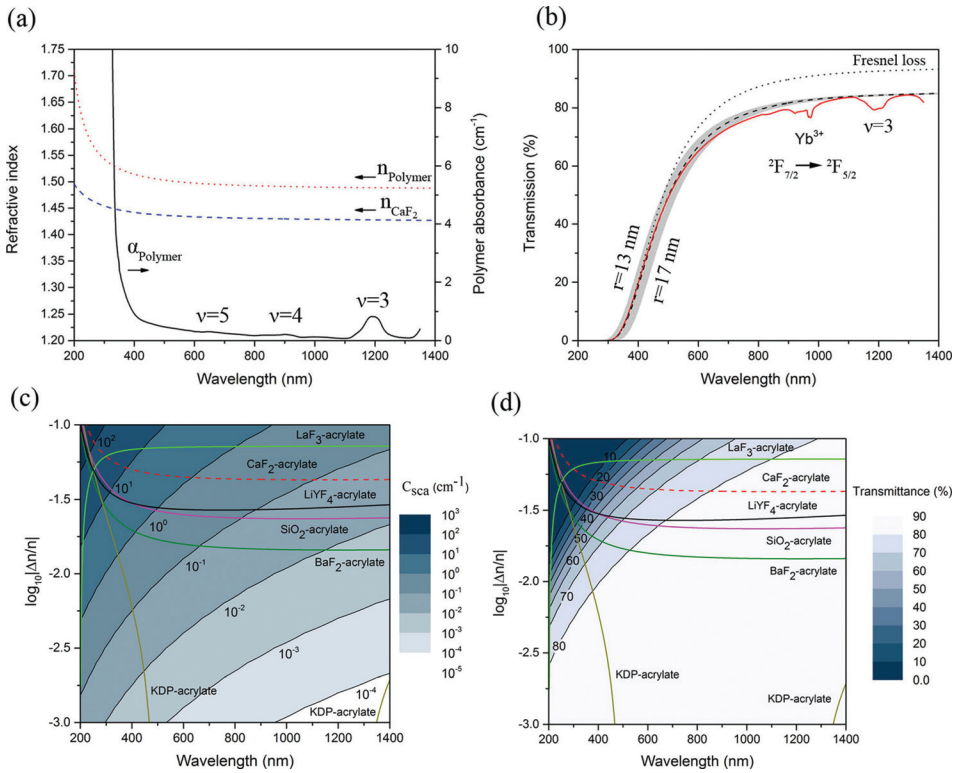

FIG. 4. (a) Optical absorbance and refractive indices of the acrylate polymer and CaF_2 as a function of wavelength. (b) Measured inline transmittance of a 2 mm-thick, 5 at. % Yb^{3+}:CaF_2-acrylate nanocomposite (solid line) and modeled transmission with (dashed line) and without (dotted line) the consideration of polymer absorption. (c) Calculated scattering cross-section as a function of refractive index mismatch and wavelength in various acrylate-based nanocomposites. (d) Calculated inline transmittance of various 2 mm-thick acrylate-based nanocomposites.

assumption may not suffice to accurately describe the scattering properties in the UV and a more detailed model might be necessary.

We have demonstrated an alternative strategy for fabricating transparent monolithic nanocomposites with inorganic loadings of up to 61 vol. % (i.e., 84 wt. % in the case of CaF_2-acrylate composites). Our approach consists in infiltrating green-bodies of random-close packed nanoparticles by organic monomers followed by a careful polymerization step. The microstructure studies presented in this work illustrate the distinct homogeneity of these materials which results from the fine porosity of the initial green-body. As per our light-scattering modeling, these characteristics ensure the effective preparation of transparent bulk-size composites even when the refractive indices of the constituents are not closely matched ($\Delta n = 6 \times 10^{-2}$). Further comprehensive investigations of the physical and mechanical properties of these materials will be carried out in the future. Because of its versatility, we foresee that this technique can be used to easily tailor the properties of nanocomposites for applications including optical sensing, low-power lasers, Christiansen filters, information storage, radiological and nuclear radiation detection, and even beyond the realm of optical materials.

The authors would like to acknowledge the personnel at the Material Characterization Facility (MCF) at the University of Central Florida, in particular, Mr. Mikhail Klimov. R.G. would like to thank CREOL and the NSTC for providing funding.

[1]H. Althues, J. Henle, and S. Kaskel, Chem. Soc. Rev. **36**, 1454 (2007).
[2]N. Tessler, V. Medvedev, M. Kazes, S. Kan, and U. Banin, Science **295**, 1506 (2002).
[3]F. Wang, Y. Han, C. S. Lim, Y. Lu, J. Wang, J. Xu, H. Chen, C. Zhang, M. Hong, and X. Liu, Nature **463**, 1061 (2010).
[4]S. Ren, L. Y. Chang, S. K. Lim, J. Zhao, M. Smith, N. Zhao, V. Bulović, M. Bawendi, and S. Gradečak, Nano Lett. **11**, 3998 (2011).
[5]J. Y. Kim, K. Lee, N. E. Coates, D. Moses, T. Q. Nguyen, M. Dante, and A. J. Heeger, Science **317**, 222 (2007).
[6]H. Zhang, Q. Bao, D. Tang, L. Zhao, and K. Loh, Appl. Phys. Lett. **95**, 141103 (2009).
[7]I. Seshadri, G. L. Esquenazi, T. Borca-Tasciuc, P. Keblinski, and G. Ramanath, Appl. Phys. Lett. **105**, 013110 (2014).
[8]W. Cai, Q. Chen, N. Cherepy, A. Dooraghi, D. Kishpaugh, A. Chatziioannou, S. Payne, W. Xiang, and Q. Pei, J. Mater. Chem. C **1**, 1970 (2013).
[9]S. Stange, E. I. Esch, M. K. Bacrania, L. O. Brown, A. J. Couture, R. E. Rico, R. D. Gilbertson, L. G. Jacobsohn, T. M. McCleskey, E. A. McKigney, R. E. Muenchausen, and R. Reifarth, in *IEEE Nuclear Science Symposium Conference Record* (2008), p. 3529.
[10]H. Schulz, L. Mädler, S. E. Pratsinis, P. Burtscher, and N. Moszner, Adv. Funct. Mater. **15**, 830 (2005).
[11]V. S. K. Chakravadhanula, M. Elbahri, U. Schürmann, H. Greve, H. T. Beyene, V. Zaporojtchenko, and F. Faupel, Nanotechnology **19**, 225302 (2008).
[12]M. Elbahri, M. K. Hedayati, V. S. K. Chakravadhanula, M. Jamali, T. Strunskus, V. Zaporojtchenko, and F. Faupel, Adv. Mater. **23**, 1993 (2011).
[13]T. Sun and J. M. Garcés, Adv. Mater. **14**, 128 (2002).
[14]Y. Cheng, C. Lü, Z. Lin, Y. Liu, C. Guan, H. Lü, and B. Yang, J. Mater. Chem. **18**, 4062 (2008).
[15]M. C. Tan, S. D. Pati, and R. E. Riman, ACS Appl. Mater. Interfaces **2**, 1884 (2010).
[16]H. Zou, S. Wu, and J. Shen, Chem. Rev. **108**, 3893 (2008).
[17]S. Kangoa, S. Kaliab, A. Cellib, J. Njugunad, Y. Habibie, and R. Kumara, Prog. Polym. Sci. **38**, 1232 (2013).
[18]S. H. Stelzig, M. Klapper, and K. Müllen, Adv. Mater. **20**, 929 (2008).
[19]P. Tao, Y. Li, R. W. Siegel, and L. S. Schadler, J. Mater. Chem. C **1**, 86 (2013).
[20]C. Liu, T. J. Hajagos, D. Kishpaugh, Y. Jin, W. Hu, Q. Chen, and Q. Pei, Adv. Funct. Mater. **25**, 4607 (2015).
[21]P. Das, J. M. Malho, K. Rahimi, F. H. Schacher, B. Wang, D. E. Demco, and A. Walther, Nat. Commun. **6**, 5967 (2015).
[22]F. Faupel, V. Zaporojtchenko, H. Greve, U. Schürmann, V. S. K. Chakravadhanula, C. Hanisch, A. Kulkarni, A. Gerber, E. Quandt, and R. Podschun, Contrib. Plasma Phys. **47**, 537 (2007).

[23]J. R. DiMaio, B. Kokuoz, and J. Ballato, J. Am. Chem. Soc. **130**, 5628 (2008).
[24]B. M. Novak, Adv. Mater. **5**, 422 (1993).
[25]A. Ikesue and Y. L. Aung, Nat. Photonics **2**, 721 (2008).
[26]N. Dong, M. Pedroni, F. Piccinelli, G. Conti, A. Sbarbati, J. E. Ramírez-Hernández, L. M. Maestro, M. C. I. Cruz, F. Sanz-Rodriguez, A. Juarranz, F. Chen, F. Vetrone, J. A. Capobianco, J. G. Solé, M. Bettinelli, D. Jaque, and A. Speghini, ACS Nano **5**, 8665 (2011).
[27]T. Kaino, M. Fujiki, and K. Jinguji, Rev. Electron. Comm. Lab. **32**, 478 (1984); T. Kaino, Jpn. J. Appl. Phys. **24**, 1661 (1985).
[28]W. Groh, Makromol. Chem. **189**, 2861 (1988).
[29]H. C. Van De Hulst, *Light Scattering by Small Particles* (Dover Publications, New York, 1981).
[30]C. F. Bohren and D. R. Huffman, *Absorption and Scattering of Light by Small Particles* (Wiley, New York, 1983).
[31]M. Quinten, *Optical Properties of Nanoparticle Systems* (Wiley-VCH Verlag GmbH & Co. KGaA, Weinheim, Germany, 2011).
[32]In a 2-constituent composite, the conversion between the volume and mass fractions, $f_{v,i}$ and $f_{m,i}$ of each phase i of density ρ_i, is $\frac{1}{f_{m,1}} = 1 + \frac{\rho_2}{\rho_1}\left(\frac{1}{f_{v,1}} - 1\right)$. The densities of CaF_2 and the acrylate polymer used in this work are 3180 and 950 kg/m^3, respectively.